Analysis of excitation and coherent amplitude enhancement of surface acoustic waves by the phase velocity scanning method

doi: 10.1063/1.355140

Analysis of excitation and coherent amplitude enhancement of surface acoustic waves by the phase velocity scanning method

Kazushi Yamanaka, O. V. Kolosov,[a] Yoshihiko Nagata, and Toshio Koda
Mechanical Engineering Laboratory, Namiki 1-2, Tsukuba, Ibaraki 305, Japan

Hideo Nishino[b] and Yusuke Tsukahara
Technical Research Institute, Toppan Printing Co., Ltd., Takanodai-Minami 4-2-3, Sugito-machi, Kitakatsushika-Gun, Saitama 345, Japan

(Received 21 April 1993; accepted for publication 16 August 1993)

We present a general theoretical formulation for the characteristics of surface acoustic waves (SAW) generated by the phase velocity scanning (PVS) method that employs a scanning single laser beam (SSB) or a scanning interference fringes (SIF). In the SSB approach, a broad band SAW pulse is generated and its amplitude is coherently enhanced when the laser scanning velocity V is equal to the phase velocity v_R of the SAW. The amplitude of the SAW follows a resonance curve represented by a sinc function of the scanning velocity V, but different spatial frequency components in the SSB significantly suppress the side lobes of the resonance curve. In the SIF approach, the scanning velocity v_f of the fringes is determined by the intersection angle and the frequency difference ω_a of the laser beams. A narrow band tone burst of SAW with frequencies higher than 100 MHz can be excited. The SAW frequency ω depends upon a characteristic time t^*, defined as a propagation time of the SAW across the laser beam spot. The SAW frequency ω is identical to the frequency difference ω_a when the laser pulse width T is longer than the characteristic time t^*. But, the SAW frequency ω is determined as a product $k_f v_R$ of the wave number of the SIF and the SAW velocity when the laser pulse width is shorter than the characteristic time. Precise frequency measurement provided by the amplitude enhancement effect and the narrow frequency bandwidth in the SIF approach make the PVS method particularly promising for the noncontact SAW velocity measurement.

I. INTRODUCTION

The noncontact generation of acoustic waves by means of a pulsed laser[1] together with noncontact detection methods[2] provides ultrasonic nondestructive evaluation (NDE) methods of elastic properties and flaws of materials in circumstances where a liquid coupler cannot be used. This laser ultrasonic method attracts much attention because of its significant potential for the NDE in hostile environments, such as high temperature, vacuum, etc. However, the main limitation of this method is its low sensitivity compared with the standard piezoelectric transducer methods. One of the reasons is the small amplitude of acoustic waves that can be generated without damage to the tested object. If one uses high peak power laser to generate strong acoustic waves, ablation damage of the surface results.[3] Even in the low peak power regime, degradation may be introduced by a repeated laser irradiation.

An approach to increase the sensitivity of the laser ultrasonic method is to improve the signal to noise ratio using a narrow bandwidth detection system. To achieve this, laser pulse is separated in time or in space using repetitive pulsing of mode locked lasers,[4] laser arrays with optical fiber delay lines,[5] and diffraction grating.[6] In these cases, trains of pulses or tone bursts of acoustic waves are generated, but the amplitude of each pulse is unchanged.

As an approach to enhance the amplitude of laser generated SAW, Cielo *et al.* proposed the converging SAW technique using a ring-shaped irradiation pattern.[7] The amplitude of the SAW at the center of the ring is enhanced due to focusing. The amplitude can be made larger than 1 nm, whereas the maximum surface temperature increase is less than 10°. However, this method reduces the efficiency in anisotropic materials because the phase matching of the SAW propagating in a different direction is not maintained.

Another method of amplitude enhancement is by the use of a scanning single laser beam (SSB).[8,9] A pulse of the SAW is generated by the SSB and it is amplified when the scanning velocity is equal to the SAW velocity. In dispersive media like plates and layered materials where the phase and group velocities are different, the role of these velocities had not been discussed. The present authors found that the scanning velocity should be equal to the phase velocity rather than the group velocity, and a tone burst of SAW is generated with duration proportional to the difference of the phase and group velocities.[10–12] Since the phase velocity plays the essential role, this method was named as the phase velocity scanning (PVS) method. Theoretical analysis of the generation of SAW[8,13] and Lamb waves[14] by the PVS method have been presented.

Although the frequency of acoustic waves generated by the SSB approach of the PVS method was limited to several MHz,[11,12] 110 MHz SAW was successfully generated

[a]On leave from Institute of Chemical Physics, Russian Academy of Science, 4 Kosygin Str., Moscow 117333, Russia.
[b]Correspondence address: Mechanical Engineering Laboratory, Namiki 1-2, Tsukuba, Ibaraki 305, Japan.

 0021-8979/93/74(11)/6511/12/$6.00

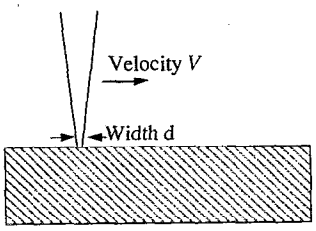

FIG. 1. Principle of phase velocity scanning (PVS) method. A scanning single beam (SSB) of laser with a width d and velocity V generates a heat pulse of a duration d/V.

by using a scanning interference fringe (SIF) formed by intersection of laser beams with different frequency.[15] The SIF approach of the PVS method is an extension of a previous method for generating bulk waves in transparent electrostrictive materials.[16] The amplitude and frequency of generated SAW were successfully controlled by changing the intersection angle of laser beams.[17] The precise frequency control is a characteristic of the SIF approach, although it is not in the SSB approach, in so far as the frequency dispersion is not significant.[10–12] In this respect, another method using static interference fringe of a short laser pulse—the laser induced grating (LIG) method[18,19]—resembles the SIF approach. But the LIG method is different from that of SIF because it uses short pulse laser beams of identical frequencies. In this situation, theoretical analysis of the SSB approach in the PVS method, the SIF, approach in the PVS method, and the LIG method based on a unified formulation are needed for a clear understanding of the advantages of each method.

In this article we present a theoretical formulation based on an approximated Green's function to systematically analyze the properties of generated SAW by the three methods mentioned above. Then, the previously obtained experimental results of the SSB[10,11] and SIF approaches[15,17] are analyzed by the same formulation. Finally, the advantages of the PVS method as a nondestructive evaluation tool are summarized following the theoretical model.

II GREEN'S FUNCTION FORMULATION FOR THERMOELASTIC GENERATION OF SAW

A. Basic principle of the phase velocity scanning (PVS) method

The basic principle of the PVS method is depicted in Fig. 1. If a laser beam is scanned along a surface of solid, absorbed energy of the laser beam at specific point P varies as a function of time as a pulse. The effective duration of this pulse and the corresponding frequency are given by $\tau=d/V$ and $F=V/d$, where d is the width of laser beam and V is the scanning velocity. This heat pulse is the driving force for generating SAW along the surface. For example, the frequency $F=3$ MHz if $V=3000$ m/s and $d=1$ mm. The amplitude of generated SAW is coherently enhanced if the scanning velocity V is equal to the phase velocity of the SAW.

The SIF are regarded as a sequence of laser beams, and each fringe is essentially similar to a SSB. However, there are important differences, since the fringe spacing can be made smaller than 30 μm, providing SAW with frequency range higher than 100 MHz. Furthermore, the number of fringes can be made quite large, providing quite narrow bandwidth necessary for high resolution.

A component of the displacement normal to the surface at position x and time t due to thermoelastic generation[1,3] of the SAW is expressed as

$$u(x,t)=\int_{-\infty}^{\infty}\int_{-\infty}^{t} G_R(x,x',t-t')s(x',t')dx'dt', \tag{1}$$

where $G_R(x,x',t-t')$ is the Green's function defined as the particle displacement at position x and time t caused by a heat pulse of delta function time dependence applied at position $x=x'$ and time $t=t'$. The Green's function for isotropic infinite plate has already been formulated and a computer program for exact solution is available.[20] The function $s(x',t')$ is the source function representing the time and spatial distribution of the laser source. Various shapes of static or scanning laser source can be expressed by $s(x',t')$.

Although the wave form of $u(x,t)$ is obtained using the numerically computed Green's function,[20] it is useful to make simple assumptions for the Green's function to investigate the behavior of different types of source function $s(x',t')$. To analyze this phenomenon readily we introduce some assumptions. First, we describe the problem in one dimension, neglecting the diffraction and excitation of bulk acoustic waves, and the surface skimming compressional waves.[21] We further assume that the Green's function has the delta function time dependence with a time delay due to propagation on solid surface as a SAW with phase velocity v_R. It is equivalent to assuming adiabatic expansion by rapid heating. Although this assumption is not suitable for describing phenomena with a long time duration, we proceed with this assumption because we are interested only in high frequency phenomena characterized by a short time duration. Then we have

$$G_R(x,x',t-t')\cong C_G\{\delta[v_R(t-t')-(x-x')] +\delta[-v_R(t-t')-(x-x')]\}, \tag{2}$$

where C_G is a coefficient including material parameters, and the detailed form is discussed later. The second term on the right hand side (r.h.s) of Eq. (2) represents SAW propagating in the $-x$ direction with velocity v_R.

B. Scanning single beam (SSB)

For a SSB with the velocity V, the source function[17] in Eq. (1) is expressed as

$$s(x',t')=AJg(x'-Vt')h_T(t'), \tag{3}$$

where A is the optical absorption coefficient, J is the peak laser power density, and $g(x')$ is its normalized spatial distribution. A finite pulse width of the laser is taken into account by the hat function $h_T(t')$ defined as

$$h_T(t')=1, \text{ where } -T/2<t'<T/2$$

$$0, \text{ otherwise.} \tag{4}$$

Let us express $g(x')$ by its Fourier transform $G(k)$ as

$$g(x')=\int_{-\infty}^{\infty} G(k)\exp(ikx')\frac{dk}{2\pi},$$

where k is the wave number representing spatial distribution. Then, the source function is expressed as the real part of

$$s(x',t')=AJ\int_{-\infty}^{\infty} G(k)\exp[ik(x'-Vt')]h_T(t')\frac{dk}{2\pi}. \tag{5}$$

Substituting Eqs. (2) and (5) into (1) we obtain

$$u(x,t)=AJC_G\int_{-\infty}^{\infty}dx'\int_{-\infty}^{t}dt'\int_{-\infty}^{\infty}G(k)\delta \times[v_R(t-t')-(x-x')]h_T(t') \times\exp[ik(x'-Vt')]\frac{dk}{2\pi}+O(-v_R),$$

where the term $O(-v_R)$ is identical to the first term except that v_R is exchanged by $-v_R$, and represents SAW propagating in the opposite direction. Integrating first with x' and then t', the result is

$$u(x,t)=AJC_GT\int_{-\infty}^{\infty}G(k)\exp[ik(x-v_Rt)] \times\operatorname{sinc}\left(\frac{k(v_R-V)T}{2}\right)\frac{dk}{2\pi}+O(-v_R), \tag{6}$$

where we assumed that $t>T/2$, i.e., the entire scanning is finished. Equation (6) represents a broad band pulse of a wave number distribution $G(k)$ and velocity v_R. The amplitude is a maximum when $V=v_R$ and it is proportional to the laser pulse width T. This is the most significant property of the SAW generated by the PVS method. By virtue of this amplitude enhancement effect, long pulse lasers of low peak intensity can be used to generate large amplitude SAW in the MHz range. This is in a sharp contrast with the conventional laser ultrasonic method[1,3] where short pulse laser of high intensity is required. This advantage of the PVS method arises from the fact that the energy of the SAW is concentrated in a small area, although the energy of laser is spatially distributed.

These features are exactly identical with the previous results obtained from other approaches.[8,10,13] The center frequency of the generated SAW pulse is given by

$$F_0=\frac{v_Rk_0}{2\pi}\cong\frac{v_R}{d}, \tag{7}$$

where k_0 is the peak wave number of $G(k)$.

C. Laser induced grating (LIG) method using a short pulse laser

Before formulating the scanning interference fringes (SIF), it is useful to formulate a related but simpler method, LIG[18,19] using a static interference fringes. The wave number of the interference fringes formed by two intersecting laser beams at the incident angle shown in Fig. 2 is given by $k_f=2K\sin\theta$, where θ is the incident angle of each laser beam onto the surface of the solid. If the angle θ is small, $k_f\cong 2K\theta$. When the pulse duration of a laser is much smaller than the period of acoustic waves, the source function can be assumed to have a time dependence of delta function. Therefore the source function is

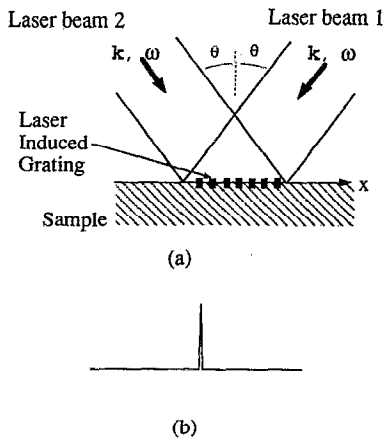

FIG. 2. Principle of the laser induced grating (LIG) method. (a) Interference fringes formed by two laser beams with identical frequencies. (b) A laser pulse of short duration.

$$s(x',t')=AJ\cos(k_fx')h_L(x')\delta(t'). \tag{8}$$

The function $h_L(x')$ is the hat function similar to Eq. (4) where L is the laser beam spot size. Although the laser produces a nonzero average heat, the dc component is neglected in Eq. (8) since we are interested in the high frequency component only. Substituting Eqs. (2) and (8) into Eq. (1) we obtain

$$u(x,t)\equiv u_L(x,t) =AJC_G\{\cos[k_f(x-v_Rt)]h_L(x-v_Rt) +\cos[k_f(x+v_Rt)]h_L(x+v_Rt)\}, \tag{9}$$

which represents two tone bursts propagating in the opposite directions. The first term is observed at $x>v_Rt-L/2$ and the second term is observed at $x<-v_Rt+L/2$, respectively. The frequency of generated SAW is given by

$$\omega=k_fv_R. \tag{10}$$

D. Scanning interference fringes (SIF)

1. A general solution

As familiar in the heterodyne interferometry, two intersecting laser beams with slightly different frequencies make SIF, as schematically shown in Fig. 3. The amplitude I of the laser beams on the surface of the specimen is expressed as

$$I=I_1\exp i[(-k_1\sin\theta)x-\omega_1t] +I_2\exp i[(k_2\sin\theta)x-\omega_2t],$$

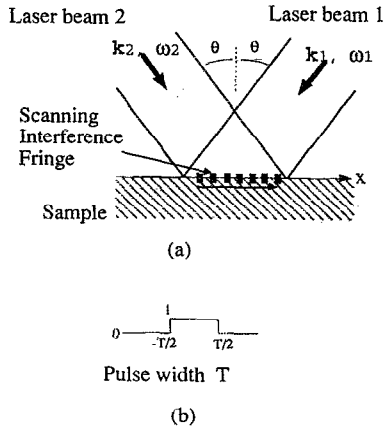

FIG. 3. Principle of the scanning interference fringes (SIF) approach of the PVS method. (a) Interference fringes formed by two laser beams with different frequencies. (b) A laser pulse of long duration

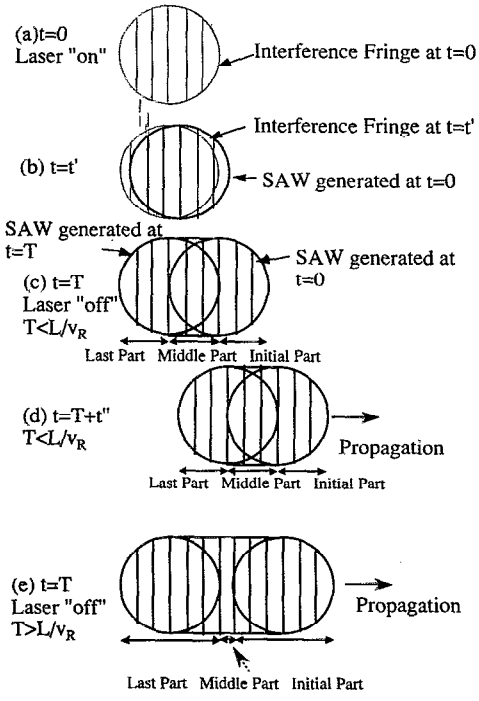

FIG. 4. Schematic illustration of generated SAW by the SIF approach. (a) Interference fringes at the time of laser switched on ($t=0$). (b) Wave front of the SAW generated at $t=0$ observed at time $t=t'$ (thick vertical lines) and SIF at the same instant (thin vertical lines). (c) Total wave front of the SAW generated during the time T where $T<L/v_R$. (d) Total SAW observed at time $t=T+t''$. The laser has already been switched off. (e) Total wave front of the SAW generated during time T where $T>L/v_R$.

where k_1,k_2,I_1,I_2 are the magnitudes of the wave number and the amplitudes of the two laser beams and amplitudes of the two laser beams. Thus, the intensity of the interference fringes are

$$I\cdot I^*=I_1^2+I_2^2+2I_1I_2\cos[(2K\sin\theta)x-\omega_a t)], \quad (11)$$

where $K\cong k_1,k_2$ is the approximate magnitude of the wave number of the laser beams, and $\omega_a=\omega_2-\omega_1$ is the frequency difference between two laser beams, respectively. The frequency difference can be introduced by a Bragg cell frequency shifter[15] or by a single laser with two oscillation frequencies. Equation (11) shows that the interference fringes are scanned along the x axis at a velocity

$$v_f=\frac{\omega_a}{2K\sin\theta} \quad (12)$$

and the wave number is

$$k_f=2K\sin\theta. \quad (13)$$

The dc component $I_1^2+I_2^2$ of Eq. (11) gives a heat pulse with a duration close to the pulse width of the laser. Since the corresponding frequency is much lower than what we are concerned with, this term is temporarily neglected in the present analysis (it is dealt with in Appendix B). The source function is then the real part of

$$s(x',t')=AJ\exp[i(k_f x'-\omega_a t')]h_L(x')h_T(t'), \quad (14)$$

where L is the laser beam spot size and T is the laser pulse width. Substituting Eqs. (2) and (14) into Eq. (1), we obtain

$$u(x,t)=AJC_G\exp[ik_f(x-v_R t)]\times\int_{-T/2}^{T/2}\exp[i(k_f v_R-\omega_a)t']\times h_L[x-v_R(t-t')]dt'+O(-v_R). \quad (15)$$

This integral gives different results depending on the pulse width of the laser T relative to the propagation time of the SAW, $t^*\equiv L/v_R$ across the laser beam spot. Figure 4 illustrates the relation of the SIF and generated SAW at various stages of the generation of the SAW by the SIF. First, (a) shows the laser beam spot within which SIF are formed. The vertical lines represent the SIF at the time $t=0$ when the laser is switched on. Next, (b) shows a part of the SAW generated at $t=0$ and observed at time $t=t'$ (thick vertical lines) as well as the SIF at the same instant (thin vertical lines). Then, (c) shows the total SAW generated from time $t=0$ to T for $T<L/v_R$. These SAW propagate while keeping the same shape after the laser is switched off as shown in (d). In (c), the initial part is defined as a part of the SAW located outside the laser beam spot. The middle part is defined as the common area of the SAW generated at $t=0$ and the laser beam spot. The last part is defined as the remaining part of above. Finally, (e) is similar to (c) for $T>L/v_R$. Note that the definition of the three parts is different from that of $T<L/v_R$ due to the change in the laser pulse width.

Let us define the case where $T>L/v_R$ as a long pulse regime and the case where $T<L/v_R$ as a short pulse regime. Relative positions of the nonzero range of the hat function in Eq. (15) for the long and short pulse regimes depend on the initial, middle, and last parts of the generated SAW in terms of the observation time t. A process to determine the integral limit of Eq. (15) is described in Appendix A and the result is listed in Table I.

TABLE I. Integral limit of Eq. (15).

Time range	Long pulse ($T > L/v_R$)	Short pulse ($T < L/v_R$)
I Initial part	$-T/2 \Rightarrow t_2$	$-T/2 \Rightarrow t_2$
II Middle part	$t_1 \Rightarrow t_2$	$-T/2 \Rightarrow T/2$
III Last part	$t_1 \Rightarrow T/2$	$t_1 \Rightarrow T/2$

2. Wave form in the middle part of the generated tone burst

Substituting the integral limit for the middle part given in Table I into Eq. (15), we find the displacement generated in the long pulse regime as

$$u(x,t) = AJC_G \exp[ik_f(x - v_R t)] \times \int_{t-(x+L/2)/v_R}^{t-(x-L/2)/v_R} \exp[i(k_f v_R - \omega_a)t']dt' + O(-v_R)$$

$$= AJC_G L/v_R \operatorname{sinc}\left(\frac{(k_f v_R - \omega_a)L}{2v_R}\right) \times \exp\left[i\omega_a\left(\frac{x}{v_R} - t\right)\right] + O(-v_R) \quad (16)$$

and in the short pulse regime as

$$u(x,t) = AJC_G \exp[ik_f(x - v_R t)] \times \int_{-T/2}^{T/2} \exp[i(k_f v_R - \omega_a)t']dt' + O(-v_R)$$

$$= AJC_G T \operatorname{sinc}\left(\frac{(k_f v_R - \omega_a)T}{2}\right) \times \exp[ik_f(x - v_R t)] + O(-v_R). \quad (17)$$

Equations (16) and (17) have a similar structure, consisting of the amplitude factor, a resonance term of a sinc function type, and a propagating sine wave term. Comparing Eqs. (16) and (B15) of Appendix B, it is shown that

$$C_G = \frac{iK\alpha}{2\rho^2 c_l^2 C X_R} \frac{v_R^2}{c_t^2}\left(\frac{1}{c_t^2} - \frac{2}{v_R^2}\right), \quad (18)$$

where ρ, c_t, c_l, K, α, and C are density, transverse and longitudinal sound velocities, bulk modulus, volumetric thermal expansion coefficient, and heat capacity of the material. The constant X_R is a function of v_R, c_t, and c_l given by Eq. (B14) of Appendix B.

When the resonance condition $k_f v_R = \omega_a$ is satisfied, the argument of the sinc function is zero, and the amplitude becomes a maximum. The controlling parameter for this condition is the wave number k_f of the SIF, which is controlled by the incident angle θ of laser beams as $k_f = 2K \sin\theta$. It is interesting to see that the frequency of the SAW is determined by the frequency difference ω_a in the long pulse regime, whereas it is determined as $\omega = k_f v_R$ in the short pulse regime, namely, a product of the wave number of SIF and SAW velocity. Although at the resonance these frequencies are identical, they differ at nonresonance condition. The long pulse regime is preferred for the precision and stability, whereas the short pulse regime provides a flexibility of variable frequency, even using a fixed frequency difference between the laser beams.

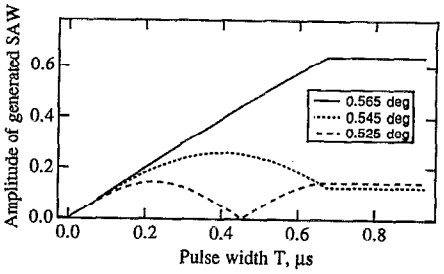

FIG. 5. Calculated amplitude of generated SAW on aluminum ($v_R = 2906$ m/s) as a function of laser pulse width at various incident angles. The angle $\theta = 0.565°$ satisfies the resonance condition and $\theta = 0.545°$ and $0.525°$ is out of resonance. A frequency difference of the laser beams is 110 MHz and the laser beam spot size is 0.5 mm.

Figure 5 shows calculated amplitude of the middle part of the generated SAW on aluminum ($v_R = 2906$ m/s) as a function of laser pulse width at various incident angles. The angle $\theta = 0.565°$ satisfies the resonance condition and $\theta = 0.545°$ and $0.525°$ are out of the resonance condition. The frequency difference of laser beams is 110 MHz and laser beam spot size is 0.5 mm. When the laser pulse width increases, the amplitude increases within the short pulse regime, and saturates at the start of the long pulse regime as shown by the solid curve. At nonresonant incident angles, the amplitude oscillates and finally reaches a constant value at the beginning of the long pulse regime as shown in the dotted and broken curves. The behavior for incident angles larger than the resonance condition, $\theta = 0.585°$ and $\theta = 0.605°$ are similar to $\theta = 0.545°$ and $0.525°$, respectively.

3. Initial and last part of the generated tone burst

From Table I it is known that the integral limits for the initial part are identical for both the short and the long pulse regime. This result is reasonable since the earliest part of the SAW wave form is generated by the earliest part of the laser pulse, which is not affected by the later part of the pulse. Therefore, the solution for the initial part should not depend on the final length of the laser pulse. Applying Table I to Eq. (15), we obtain for the initial part

$$u(x,t) = \frac{iAJC_G}{k_f v_R - \omega_a}\left\{\exp\frac{-i(k_f v_R - \omega_a)T}{2} \times \exp[ik_f(x - v_R t)] - \exp\frac{i(k_f v_R - \omega_a)L}{2v_R} \times \exp\left[i\omega_a\left(\frac{x}{v_R} - t\right)\right]\right\} + O(-v_R) \quad (19)$$

and for the last part

$$u(x,t)=\frac{-iAJC_G}{k_f v_R-\omega_a}\left\{\exp\frac{i(k_f v_R-\omega_a)T}{2}\right.$$
$$\times\exp[ik_f(x-v_R t)]$$
$$\left.-\exp\frac{-i(k_f v_R-\omega_a)L}{2v_R}\exp\left[i\omega_a\left(\frac{x}{v_R}-t\right)\right]\right\}$$
$$+O(-v_R). \tag{20}$$

In both cases, a beat signal is observed out of the resonance condition ($k_f v_R \neq \omega_a$), because Eqs. (19) and (20) are the sum of two harmonic waves with different frequencies. The number of beats increases as the nonresonance condition proceeds.

The envelope of the beat signal propagates with the group velocity v_G of the SAW, whereas the carrier itself propagates with the phase velocity v_P. If the SAW are dispersive, v_P and v_G are different and the wave form of Eqs. (19) and (20) changes as it propagates. This leads to the possibility of evaluating both v_P and v_G from the measurement of the wave form at two different positions, by introducing the out of resonance condition $k_f v_R \neq \omega_a$.

To find an asymptotic form to the limit of resonance, Eq. (19) is rewritten as

$$u(x,t)=AJC_G\exp[i(k_f x-\omega_a t)]\left\{\exp\left[-i\Delta\omega\left(t-\frac{T}{2}\right)\right]\right.$$
$$\left.-\exp\left[i\Delta\omega\left(\frac{L}{2v_R}-\frac{x}{v_R}\right)\right]\Big/-i\Delta\omega\right\}+O(-v_R), \tag{21}$$

where $\Delta\omega=k_f v_R-\omega_a$. It is easy to see that (21) represents an oscillation of frequency ω_a, with amplitude modulation at a frequency of $\Delta\omega$. If $\Delta\omega$ is small, the exponential term of (21) is expanded to first order and we obtain

$$u(x,t)\cong AJC_G\exp[i(k_f x-\omega_a t)]$$
$$\times\left\{t-\left[\frac{x}{v_R}-\frac{1}{2}\left(\frac{L}{v_R}+T\right)\right]\right\}+O(-v_R). \tag{22}$$

This equation indicates that, at or near the resonance, the initial part of the signal is a tone burst whose amplitude is growing linearly with time. The first signal arrives at time

$$t=\frac{x}{v_R}-\frac{1}{2}\left(\frac{L}{v_R}+T\right). \tag{23}$$

Similarly, for the last part, a solution of linearly decaying tone burst is obtained as

$$u(x,t)=AJC_G\exp[i(k_f x-\omega_a t)]$$
$$\times\left[v_R x+\frac{1}{2}\left(\frac{L}{v_R}+T\right)-t\right]+O(-v_R). \tag{24}$$

It is in contrast to the middle part, where the amplitude is constant in time.

Figure 6 shows calculated tone burst of SAW for the short pulse regime including the initial, middle, and last part. In this example, the frequency difference of laser beams is assumed to be 110 MHz, laser pulse width is 140 ns, and laser beam spot size is 0.5 mm. The upper curve is obtained at the resonance condition ($\theta=0.565°$). The lower curve is obtained at the nonresonance condition ($\theta=0.525°$), and it is characterized by the beating at the initial and last part.

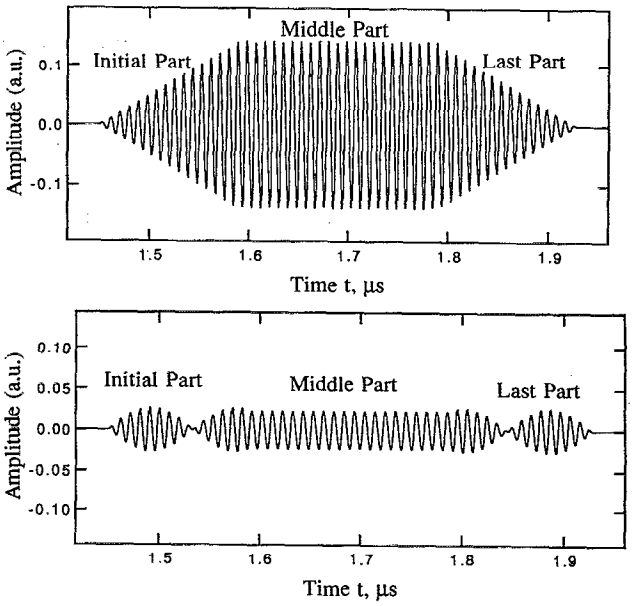

FIG. 6. Calculated wave form of the SAW for the short pulse regime of the SIF approach. A frequency difference of the laser beams is 110 MHz, the laser pulse width is 140 ns, and the laser beam spot size is 0.5 mm. The upper curve shows the resonance condition (0.565°) and the lower curve shows out of the resonance condition (0.525°) with a beating.

In practice, the spatial distribution of heat in the laser spot may not have a hat function profile but a graded profile. In this case, the above described features of the initial and last parts are mixed with that of the middle part. Consequently, the beating at the nonresonance condition may be observed not only in the initial and last part but also in the middle part.

So far, we used the approximated Green's function to gain insight into the coherent amplitude enhancement of the SAW by the PVS method. However, more exact derivation is also possible by directly solving the thermal and elastic wave equations as shown in Appendix B. This derivation gives an absolute value for the amplitude of the SAW.

III. COMPARISON WITH EXPERIMENTS

A. Experimental setup

The experimental setup to generate SAW by the SSB approach is essentially identical to our previous work for generating single mode Lamb waves.[10–12] In Fig. 7(a), a flash lamp pumped Nd:YAG laser beam with pulse width T of 2 ms was deflected using a polygon laser scanner with a maximum rotation speed of 24 000 rpm. The laser beam was focused onto a rectangular spot with length d of 10 mm and width d of 0.5–1 mm using a cylindrical lens with focal length f of 600 mm. The scanning velocity V was

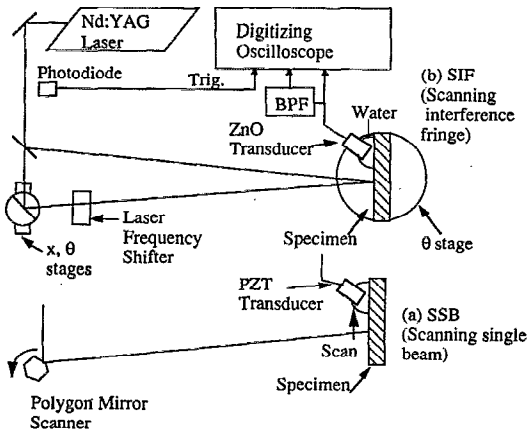

FIG. 7. Experimental setup for the (a) SSB and (b) SIF approach in the PVS method. BPF stands for a band pass filter.

controlled by varying the rotation speed of the mirror. The scanning length L of the beam was varied by using a mask. The acoustic waves were detected using a piezoelectric transducer with a surface wave wedge attached to the sample. The center frequency and 6 dB bandwidth were 2.23 and 1.18 MHz, respectively.

To trigger the YAG laser synchronously with the rotation of the mirror, an index pulse was generated using a He-Ne laser beam reflected from the faces of the polygon mirror. The index pulse was then frequency divided and a trigger pulse of 1–2 Hz repetition was obtained. By using this trigger pulse it was ensured that the observed acoustic waves are generated by a fraction of the long laser pulse reflected by the same face of the polygon mirror. Such a synchronous triggering method, with respect to the rotation of mirror, was essential for excellent stability and reproducibility of observed wave forms.

Figure 7(b) shows the experimental setup used for the SIF approach.[15,17] Two laser beams with a frequency difference were used to generate the SIF. The laser was a second harmonic Q-switched Nd:YAG laser (532 nm) with a long cavity length of 2 m, which enabled a long pulse width of 140 ns. The frequency difference of 110 MHz was introduced by a laser frequency shifter made of a TeO_2 Bragg cell.

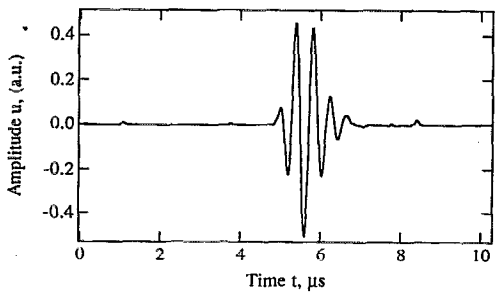

FIG. 8. A SAW pulse on aluminum sample generated by the SSB approach.

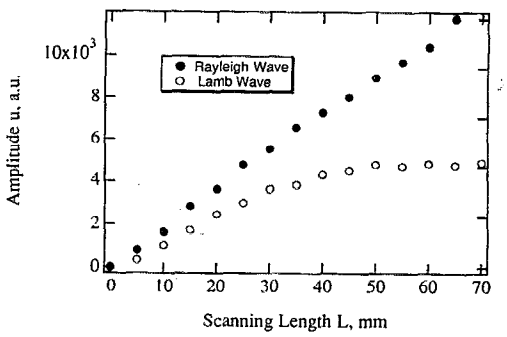

FIG. 9. Amplitude of the experimentally observed SAW pulse (closed circles) and Lamb wave pulse as a function of the laser scanning length in the SSB approach.

B. SAW generated by the SSB approach

On a 6-mm-thick aluminum sample, a broad band pulse of unidirectional SAW was observed. The duration of generated pulse tended to decrease and the amplitude increased as the scanning velocity V approached v_R.[11,12] Figure 8 is an observed SAW pulse on the aluminum sample generated by the SSB approach at the scanning velocity $V=v_R$ (2906 m/s) and the scanning length $L=65$ mm.

To verify the amplitude enhancement effect, the amplitude of the peak at $V=v_R$ is plotted as a function of the scanning length L as closed circles in Fig. 9. The theoretically predicted linear amplitude enhancement was clearly observed. Since the linearity was maintained, even at the maximum scanning length of $L=65$ mm, further increase in the amplitude is expected if L is further increased. For comparsion, the amplitude of the Lamb wave, on a plate with the thickness, width, and length of the plate 1.5, 60, and 120 mm, was plotted as an open circle. Even for the Lamb waves with velocity dispersion, the amplitude enhancement was observed for the scanning length of 0–40 mm. However, a saturation of the amplitude was observed at a scanning length of more than that. This is due to the existence of group velocity dispersion.[10–12,14]

The power spectra of the SAW pulse was evaluated and shown in Fig. 10. The peak frequency F_0 was located around 2.2 MHz and is compatible with the theoretically predicted value of 2.96 MHz using Eq. (7) with $d=1$ mm and $v_R=2906$ m/s. Except for the small ripples observed for some velocities, the peak frequency and the bandwidth of the spectra remained constant when the scanning velocity was changed. This is in contrast with the previously

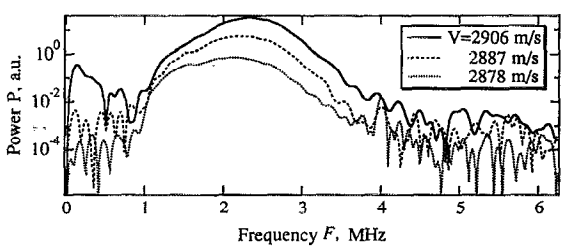

FIG. 10. Power spectra of SAW pulse generated at different scanning velocity in the SSB approach.

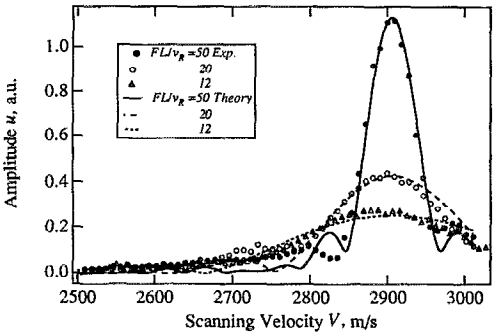

FIG. 11. Amplitude of SAW pulse generated by the SSB approach as a function of scanning velocity in the SSB approach.

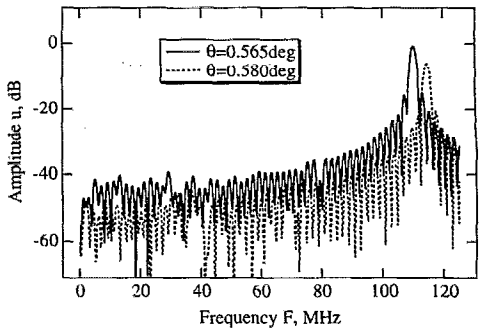

FIG. 13. Power spectra of SAW tone burst generated by the SIF approach at the resonance (0.565°) and out of the resonance (0.580°) conditions.

reported result on Lamb waves,[10–12,14] where the peak frequency varied as the scanning velocity varied according to the phase velocity dispersion curve.

The curves in Fig. 11 show the calculated amplitude of the SAW pulses by Eq. (7) as a function of the scanning velocity for the scanning lengths $L=65$, 25, and 15 mm. Each curve is labeled by the figure of merit

$$m=F_0L/v_R. \tag{25}$$

It is seen that the width of the resonance peaks decreases and the magnitude increases as m is increased.

The peak to peak amplitude of the experimentally observed SAW pulses are also plotted by circles and triangles in Fig. 11.[11,12] The peak of the data for $m=50$ was normalized to coincide with the theoretical curve. The other data agreed with theoretical curves for $m=20$ and 12 with the same normalization factor. The agreement was excellent for the height and width of the main resonance peak near $V=v_R$.

The theoretical model can be simplified to a single frequency model. When the integration over k in Eq. (7) is removed and k was set to the peak wave number k_0, a simple sinc function is obtained. It is interesting to note that the main peak in Fig. 11 was essentially unchanged, although significant side lobes appeared. (A similar curve will be shown later for the SIF approach in Fig. 15). Since, in most applications, only the main peak is important where significant amplitude enhancement of SAW takes place, the single frequency model is also useful and the figure of merit m is a reliable criterion for evaluating the performance of the PVS method. However, the suppression of side lobes is important with respect to the directivity. The magnitude of the wave propagating in the opposite direction is estimated to be -40 dB from higher order side lobes in a sinc function near $V=-v_R$. However, the magnitude is much less than this estimate due to the suppression of side lobes in the broad band model used in Fig. 11. In fact, SAW propagating in the opposite direction were never observed in the present experiment.

C. SAW generated by the SIF approach

The experiments of the SIF method were carried out in a short pulse regime. Figure 12 is a typical SAW tone burst generated by the SIF approach on aluminum with a laser frequency difference of 110 MHz.[15] The laser beam spot size was 2 mm. Since the number of carriers is quite large, the frequency spectra have narrow peaks as shown in Fig. 13. A remarkably large signal to noise (S/N) ratio is noticed. Closed circles in Fig. 14 show the peak frequency of the spectra as a function of the incident angle of the laser beam.[17] The solid line represents the calculated frequency of SAW, using Eq. (10). The excellent agreement between the experimental data and calculated line indicates that the frequency of SAW is not defined by the frequency shift of the laser but by the SAW velocity and the spacing of the SIF in the short pulse regime.

The accurate frequency measurement is advantageous in SAW velocity measurements. From the slope of the fitted line to the experimental data of frequency and angle in Fig. 14, SAW velocity may be accurately determined. If

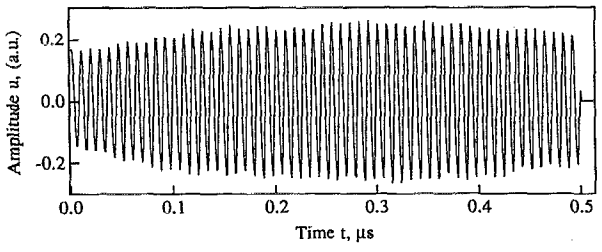

FIG. 12. Typical wave form of SAW tone burst generated by the SIF approach on aluminum with the laser frequency difference of 110 MHz. The laser beam spot size was 2 mm.

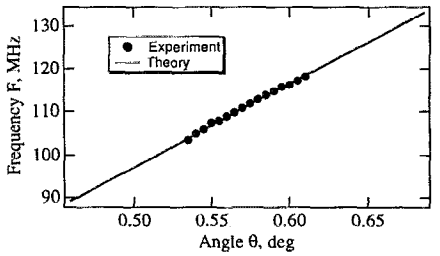

FIG. 14. Peak frequency of the SAW tone burst as a function of the laser beam incident angles.

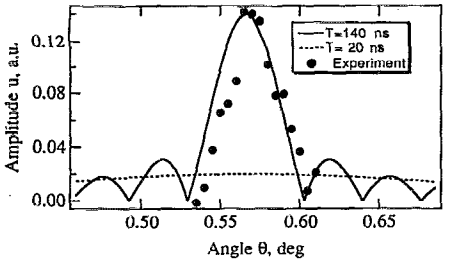

FIG. 15. Resonance curve for the SIF approach. Amplitude of the SAW pulse generated by SIF as a function of the incident angle of lasers.

the media is dispersive, the dispersion curves[10–12,14] can be obtained. By adjusting the frequency difference of the laser beams, measurable frequency range is increased and the SAW velocity is determined as a ratio of the measured frequency of the SAW and the wave number of the SIF determined from the incident angle. It will give a new and accurate method for quantitative nondestructive evaluation of elastic property of materials in microscopic scale.

The most important implication of Eq. (17) is that the amplitude of SAW is linearly proportional to the laser pulse width T. The solid curve in Fig. 15 shows a resonance curve for the laser pulse width $T=140$ ns using Eq. (17). The dotted curve is the resonance curve for the laser pulse width $T=20$ ns. The peak amplitude is seven times smaller than that for $T=140$ ns. The experimental results for the amplitude of generated SAW for each different incident angle are also shown in Fig. 15 by the closed circles.[17] When the incident angle was different from the resonance condition by more than 0.05°, the amplitude of the generated SAW was too small for accurate frequency measurements. The agreement between the experimental data and theoretical curve is acceptable, although the experimental data were slightly shifted to the right of the theoretical curve due to an insufficient alignment of the optical setup.

IV. DISCUSSIONS

A. Amplitude enhancement in the PVS method

The most significant difference between the LIG method described by Eq. (9) and the PVS method described by Eqs. (6), (16), and (17) is the amplitude factor. The amplitude is proportional to the beam spot size L in the long pulse case of SIF. In the short pulse regime, the amplitude of the SAW is enhanced during the scanning of the fringes, and it is proportional to the laser pulse width T. The LIG method is regarded as a limiting case of $T\to 0$ and there is no amplitude enhancement effect.

A relation between the SIF approach and the LIG method is also derived in more general form. Using the displacement induced by the LIG in Eq. (9), we can write

$$u_L(x,t-t')=AJC_G\exp[i(k_f x-\omega t+\omega t')]\times h_L[x-v_R(t-t')]+O(-v_R). \quad (26)$$

Comparing (15) with (26) we find

$$u(x,t)=\int_{-T/2}^{T/2} u_L(x,t-t')\exp(i\omega t')dt'. \quad (27)$$

This equation indicates that the displacement induced by the SIF is expressed as a superposition of the displacement made by the LIG with appropriate time dependent phase shift.

The amplitude of the SAW generated by the LIG method is determined by the peak power density of the laser. Then, if one tries to generate large amplitude SAW, the surface of the specimen is sometimes damaged by the laser ablation due to large peak power density. The feature of the amplitude enhancement effect of generated SAW brings a high signal to noise ratio essential for precise and reliable measurements.

B. Directivity

SAW generated by standard laser ultrasonic methods[1] propagates towards many directions. Even if an elongated stripe of the laser beam spot is used, the SAW propagates to two opposite directions. Then in a small object with reflecting boundaries, there might be the problem of unwanted multiple echoes which disturb the SAW to be observed. In the PVS method, in contrast, this problem is minimized because propagation of the SAW is restricted to only one direction. The amplitude of the SAW propagating in the opposite direction is evaluated by substituting $v_R=-v_R$ in Eq. (6). This wave is more than 40 dB smaller than the forward propagating wave, provided that $m=50$.

Although bulk longitudinal and shear acoustic waves are generated by each fringe, the acoustic waves whose amplitude is coherently enhanced at the resonance condition are only the SAW. This situation may be compared with the excitation of leaky SAW by the critical angle method in acoustic microscopy and liquid immersion ultrasonics.

C. Requirement of laser

Although the frequency of the SAW generated by the LIG method can also be changed by adjusting the intersection angle of the laser beams, the highest frequency is limited by the laser pulse width. Consequently, in order to generate SAW with a frequency higher than 100 MHz, one is forced to employ lasers with pulse width shorter than 5 ns, mostly mode locked picosecond lasers, whereas in SIF only a high frequency Bragg cell is needed.

V. CONCLUSION

All the principal features of the phase velocity scanning (PVS) method, which were experimentally observed, are successfully described by a simple Green's function analysis. A short pulse of SAW is generated by a scanning single beam (SSB) when the scanning velocity is equal to the SAW velocity. The amplitude of the SAW follows a sinc function type resonance curve, but a wide bandwidth inherent in the SSB approach significantly reduces the side lobe level of the resonance curve.

In the SIF approach, the scanning velocity of the fringes is controlled by the intersection angle of two laser

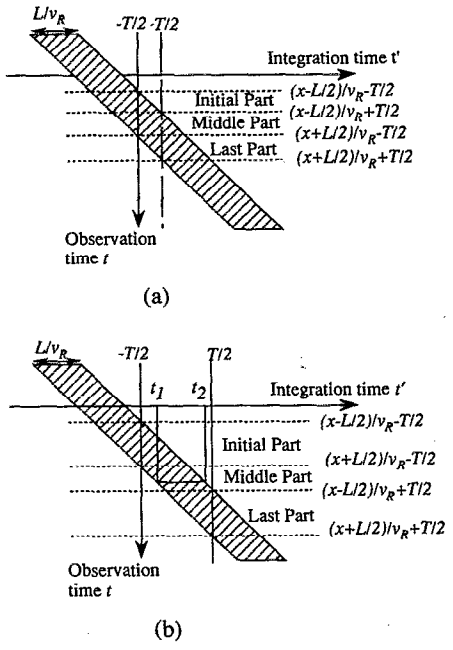

FIG. 16. Diagram to determine the integral limit of Eq. (15): (a) short pulse regime, (b) long pulse regime.

beams with a frequency difference. In contrast to the SSB, generated SAW has a shape of tone burst and the frequency can be arranged to be above 100 MHz, which is necessary for characterizing thin surface layers. If the laser pulse width is smaller than the propagation time of the SAW along the laser spot, the frequency is determined not by the frequency difference of the laser beams but by the SAW velocity divided by the spacing of SIF. The SAW generated by the SIF approach can be regarded as an integration of SAW generated by the laser induced grating method using very short pulsed lasers. The amplitude of SAW follows a sinc function type resonance curve. The amplitude enhancement at the resonance condition brings directivity and high signal to noise ratio essential for precise and reliable measurements. Therefore, the SIF approach of the PVS method will find many applications in the characterization of micromechanical properties of materials and components.

APPENDIX A. INTEGRAL LIMITS FOR EQ. (15) REPRESENTING EACH PART OF THE TONE BURST

Relative position of a nonzero range of the hat function in Eq. (15) for the short pulse regime and long pulse regime are shown in Fig. 16. The integral limit in (15) corresponds to the hatched area, a nonzero range of $h_L[x-v_R(t-t')]$, between the two lines $t'=-T/2$ and $t'=T/2$. Referring to Fig. 16, the integral limits for the initial, middle, and last parts are obtained in terms of the observation time t.

In Fig. 16, t_1 and t_2 are defined as

$$t_1 \equiv t-\frac{x+L/2}{v_R}, \qquad t_2 \equiv t-\frac{x-L/2}{v_R}. \tag{A1}$$

The borders of all three parts are also shown. Referring to this figure, integral limits in (15) are obtained as listed in Table I.

APPENDIX B. EXACT DERIVATION OF THE DISPLACEMENT OF THE SAW GENERATED BY THE SIF

We start from basic equations for the displacement vector $\mathbf{u}$ and for the temperature variation T

$$\rho\frac{\partial^2 u_i}{\partial t^2}=\rho c_t^2\nabla^2 u_i+\rho(c_l^2-c_t^2)\frac{\partial}{\partial x_i}(\nabla\cdot u)-K\alpha\frac{\partial T}{\partial x_i} \quad (i=1,2,3),$$
$$\rho C\frac{\partial T}{\partial t}-\kappa\nabla^2 T=Q(t,x), \tag{B1}$$

where u_i and x_i are the ith components of $\mathbf{u}$ and the coordinate vector, $\mathbf{x}$, respectively, and κ is the thermal conductivity of the solid material. The other constants are defined in the main text. The bulk modulus is related to the sound velocities and the density,

$$K=\rho\left(c_l^2-\frac{4}{3}c_t^2\right). \tag{B2}$$

$Q(t,\mathbf{x})$ is a spatial distribution of the heat generation rate.

We assume that the solid occupies a half space with $x_3>0$, and a vacuum with $x_3<0$. Boundary conditions are that the solid surface is stress free and there is no heat flow across the surface. Thus, at $x_3=0$,

$$\frac{\partial u_i}{\partial x_3}+\frac{\partial u_3}{\partial x_i}=0, \quad \text{for } i=1,2,$$
$$(c_l^2-2c_t^2)\left(\frac{\partial u_1}{\partial x_1}+\frac{\partial u_2}{\partial x_2}\right)+c_l^2\frac{\partial u_3}{\partial x_3}-\frac{K\alpha}{\rho}T=0, \tag{B3}$$
$$\frac{\partial T}{\partial x_3}=0.$$

As shown in Fig. 3, two laser beams illuminate the solid surface to form a heat source within the skin depth of the solid, which, in turn, generates ultrasonic waves going away from the surface. Thus, the heat generation rate is

$$Q(t,x)=\mu e^{-\mu x_3}g(t,\mathbf{r}), \tag{B4}$$

where μ is an inverse of the skin depth and $\mathbf{r}$ is a two-dimensional vector (x_1,x_2). The function $g(t,\mathbf{r})$ is the heat generation rate per unit area. Hereafter we assume that the width of the laser beams is sufficiently larger than the wave length of the interference fringes, so that we regard it as a one-dimensional problem. The interference fringes are assumed to extend from $-L/2$ to $L/2$ in x_1 direction, and turn on during $-T/2<t<T/2$. Then, the heat generation rate in a unit surface caused by the SIF is

$$g(t,\mathbf{r})=[1+\cos(\omega_a t-k_f x_1)]AJh_L(x_1)h_T(t), \quad \text{(B5)}$$

where the functions h_L and h_T are hat functions defined by Eq. (4).

Following the procedure in previous papers[13,14] the component of the displacement whose movement is normal to the surface at $x_3=0$ is derived from (A1) and (B1) with boundary conditions (B3),

$$u_3(t,x_3=0) = \int_{-\infty}^{+\infty}\frac{d\omega}{2\pi}\int_{-\infty}^{+\infty}\frac{d^2k}{(2\pi)^2}e^{-i\omega t+i\mathbf{k}\cdot\mathbf{r}} \times\tilde{u_3}(\omega,x_3=0), \quad \text{(B6)}$$

where

$$\tilde{u_3}(\omega,x_3=0)=-\frac{k_t^2(k_t^2-2k^2)}{R(\omega,k)}\tilde{S}(\omega,k)\tilde{g}(\omega,k), \quad \text{(B7)}$$

$$\tilde{S}(\omega,k)\rightarrow\frac{iK\alpha}{\rho^2c_t^2C}\frac{1}{\omega}, \quad (\mu\rightarrow\infty,\kappa\rightarrow 0), \quad \text{(B8)}$$

$$R(\omega,k)=(q_t^2-k^2)(k_t^2-2k^2)+4k^2q_lq_t, \quad \text{(B9)}$$

and

$$q_t=\sqrt{k_t^2-k^2}, \quad k=\sqrt{\mathbf{k}^2}, \quad k_t=\omega/c_t, \quad q_l=\sqrt{k_l^2-k^2}.$$

Approximation in (B8) corresponds to neglecting the skin depth and thermal diffusion length and assuming that the laser power is converted to the stress at the solid surface. This is equivalent to approximating the Green's function by the delta function in Eq. (2) in Sec. IIA. Although this assumption is not suitable to describe phenomena with a long time duration, we proceed with this assumption in the following because we are interested only in high frequency phenomena characterized by a short duration of time. The Fourier transform of $g(t,\mathbf{r})$ is

$$\tilde{g}(\omega,k)=2\pi AJ\delta(k_2)[\tilde{h_T}(\omega)\tilde{h_L}(k_1) +\tfrac{1}{2}\tilde{h_T}(\omega+\omega_a)\tilde{h_L}(k_1+k_f) +\tfrac{1}{2}\tilde{h_T}(\omega-\omega_a)\tilde{h_L}(k_1-k_f)], \quad \text{(B10)}$$

where

$$\tilde{h_L}(k_1)=L\,\mathrm{sinc}\left(\frac{k_1L}{2}\right). \quad \text{(B10)}$$

Substitution of (B7)–(B11) into (B7) gives us the surface displacement

$$u_3(x_3=0)=-AJ_iF\int_{-\infty}^{+\infty}\frac{d\omega}{2\pi}\int_{-\infty}^{+\infty}\frac{dk_1}{2\pi}e^{-i\omega t+ik_1x_1} \times\frac{k_t^2(k_t^2-2k^2)}{R(\omega,k)\cdot\omega}[\tilde{h_T}(\omega)\tilde{h_L}(k_1) +\tfrac{1}{2}\tilde{h_T}(\omega+\omega_a)\tilde{h_L}(k_1+k_f) +\tfrac{1}{2}\tilde{h_T}(\omega-\omega_a)\tilde{h_L}(k_1-k_f)], \quad \text{(B11)}$$

where F is a numerical factor depending on materials constants,

$$F=\frac{iK\alpha}{\rho^2c_l^2C}. \quad \text{(B12)}$$

We concentrate here on the SAW generation, so that we neglect all the singularities except for the SAW poles coming from the zeros of $R(\omega,k)$. First, we integrate with respect to k assuming that $x>L/2$, that is the observation of the displacement is made outside of the laser illuminated area in the same direction as the scanning of interference fringe. After manipulation, we have

$$u_3(x_3=0) =\frac{-iAJF}{2X_R}\frac{v_R^2}{c_t^2}\left(\frac{1}{c_t^2}-\frac{2}{v_R^2}\right)\Bigg[\int d\xi\,h_T\left(t-\frac{x_1}{v_R}-\xi\right)h_{L/v_R}(\xi) +\frac{1}{2}e^{i\omega_a[t-(x_1/v_R)]}\int d\xi\,e^{-i\xi(\omega_a-v_Rk_f)}h_T\left(t-\frac{x_1}{v_R}-\xi\right) \times h_{L/v_R}(\xi)+\frac{1}{2}e^{-i\omega_a[t-(x_1/v_R)]}\int d\xi\,e^{i\xi(\omega_a-v_Rk_f)} \times h_T\left(t-\frac{x_1}{v_R}-\xi\right)h_{L/v_R}(\xi)\Bigg], \quad \text{(B13)}$$

where

$$X_R=\left[8-\left(\frac{v_R^2}{c_t^2}-2\right)\left(\frac{v_R^4}{c_t^4}-2\frac{v_R^2}{c_t^2}-4\right)\frac{c_l^2}{c_t^2}\right]\Big/c_l^2\left(\frac{c_l^2}{c_t^2}-2\right) \quad \text{(B14)}$$

and v_R is the SAW velocity. Let us assume for the long pulse regime, $T>L/v_R$, that the duration of the laser pulse is longer than the time necessary for the SAW to travel across the illuminated area. The integrals in the square bracket in (B14) are carried out in three different cases shown in Appendix A.

In the middle part of the pulse where $-T/2+L/(2v_R)<t-x_1/v_R<T/2-L/(2v_R)$, either of the hat functions is zero except for a region where $t-x_1/v_R-L/(2v_R)<x<t-x_1/v_R+L/(2v_R)$. Then the integration is carried out

$$u_3(x_3=0) =\frac{-iAJFL}{2X_Rv_R}\frac{v_R^2}{c_t^2}\left(\frac{1}{c_t^2}-\frac{2}{v_R^2}\right) \times\left[1+\mathrm{sinc}\left(\frac{L(\omega_a-k_fv_R)}{2v_R}\right)\cos\left(\omega_at-\omega_a\frac{x_1}{v_R}\right)\right]. \quad \text{(B15)}$$

The high frequency component of this equation is equivalent to Eq. (16) of Sec. IID 2 provided that the coefficient C_G is given by Eq. (18).

[1] D. A. Hutchins, in *Physical Acoustics*, Vol. XVIII, edited by W. P. Mason and R. N. Thurston (Academic, San Diego, 1988), pp. 21–123.
[2] J. P. Monchalin, IEEE Trans. Ultrason. Ferroelectronics, Frequency Control **UFFC-33**, 485 (1986).
[3] J. D. Aussel, A. Le. Burn, and J. C. Baboux, Ultrasonics **26**, 245 (1988).

[4] J. B. Deaton, Jr., A. D. W. Mckie, J. B. Spicer, and J. W. Wagner, Appl. Phys. Lett. **56**, 2390 (1990).
[5] J. Jarzynski and Y. H. Berthelot, J. Acoust. Soc. Am. **85**, 158 (1989).
[6] J. Huang, S. Krishnaswamy, and J. D. Achenbach, J. Acoust. Soc. Am. **92**, 2527 (1992).
[7] P. Cielo, F. Nadeau, and M. Lamontagne, Ultrasonics **23**, 55 (1985).
[8] A. M. Dykhne and B. P. Rysev, Poverkh. Fiz. Khim. Mekh. **6**, 17 (1983).
[9] E. P. Velikhov, E. V. Dan'shchikov, V. A. Dymshakov, A. M. Dykhne, F. V. Levedev, V. D. Pis'mennyl, and A. V. Ryazanov, Pis'ma Zh. Eksp. Teor. Fiz. **38**, 483 (1983) [JETP Lett. **38**, 584 (1983)].
[10] K. Yamanaka, Y. Nagata, and T. Koda, Appl. Phys. Lett. **58**, 1591 (1991).
[11] K. Yamanaka, Y. Nagata, and T. Koda, in *Review of Progress in Quantitative Nondestructive Evaluation*, Vol. 11, edited by D. O. Thompson and D. E. Chimenti (Plenum, New York, 1992), p. 633.
[12] K. Yamanaka, Y. Nagata, and T. Koda, Nondestr. Test. Eval. **8-9**, 37 (1992).
[13] Y. Tsukahara, Proceedings of the 1992 IEEE Ultrasonics Symposium, p. 589.
[14] Y. Tsukahara, Appl. Phys. Lett. **59**, 2384 (1991).
[15] H. Nishino, Y. Tsukahara, Y. Nagata, T. Koda, and K. Yamanaka, Appl. Phys. Lett. **62**, 2036 (1993).
[16] D. E. Caddes, C. F. Quate, and C. D. W. Wilkinson, Appl. Phys. Lett. **8**, 309 (1966).
[17] H. Nishino, Y. Tsukahara, Y. Nagata, T. Koda, and K. Yamanaka, Jpn. J. Appl. Phys. **32**, 2536 (1993).
[18] G. Cachier, Appl. Phys. Lett. **17**, 419 (1970).
[19] A. Harata, H. Nishimura, and T. Sawada, Appl. Phys. Lett. **57**, 132 (1990).
[20] N. N. Hsu, NBS special report, NBSIR 85-3234 (1985).
[21] J. Kushibiki and N. Chubachi, IEEE Trans. **SU-32**, 189 (1985).